

---

# Efficient Refusal Ablation in LLM through Optimal Transport

---

Geraldin Nanfack<sup>1,2</sup> Eugene Belilovsky<sup>1,2</sup> Elvis Dohmatob<sup>1,2</sup>

## Abstract

Safety-aligned language models refuse harmful requests through learned refusal behaviors encoded in their internal representations. Recent activation-based jailbreaking methods circumvent these safety mechanisms by applying orthogonal projections to remove refusal directions, but these approaches treat refusal as a one-dimensional phenomenon and ignore the rich distributional structure of model activations. We introduce a principled framework based on optimal transport theory that transforms the entire distribution of harmful activations to match harmless ones. By combining PCA with closed-form Gaussian optimal transport, we achieve efficient computation in high-dimensional representation spaces while preserving essential geometric structure. Across six models (Llama-2, Llama-3.1, Qwen-2.5; 7B-32B parameters), our method achieves up to 11% higher attack success rates than state-of-the-art baselines while maintaining comparable perplexity, demonstrating superior preservation of model capabilities. Critically, we discover that layer-selective intervention—applying optimal transport to 1-2 carefully chosen layers at approximately 40-60% network depth—substantially outperforms full-network interventions, revealing that refusal mechanisms may be localized rather than distributed. Our analysis provides new insights into the geometric structure of safety representations and suggests that current alignment methods may be vulnerable to distributional attacks beyond simple direction removal.

## 1. Introduction

Large language models (LLMs) have achieved remarkable capabilities across diverse tasks (Brown et al., 2020; Chowdhery et al., 2023; Bai et al., 2022), but concerns about their

<sup>1</sup>Concordia University, Montreal, Canada <sup>2</sup>Mila – Quebec AI Institute, Montreal, Canada. Correspondence to: Geraldin Nanfack <geraldin.nanfack@concordia.ca>.

Preprint. March 5, 2026.

potential to generate harmful content have spurred extensive efforts in safety alignment (Bai et al., 2022; Ouyang et al., 2022). Modern alignment techniques, such as reinforcement learning from human feedback, successfully reduce the likelihood of generating harmful outputs by encoding refusal behaviors in model representations (Rafailov et al., 2023; Wu et al., 2024; Rafailov et al., 2023). However, recent work has revealed that these safety mechanisms can be circumvented through targeted manipulation of prompts or internal model representations, raising important questions about the robustness of current alignment approaches (Arditi et al., 2024; Schwinn et al., 2024; Dunefsky & Cohan, 2025).

Known as jailbreaking techniques, these adversarial manipulations bypass LLM refusal and have evolved through two distinct threat models. Initially, attacks operated at the prompt level, where adversaries craft malicious inputs—for instance, by appending adversarial suffixes (Zou et al., 2023b; Andriushchenko et al., 2025)—without necessary access to model internals. However, the widespread release of open-source weights for safety-aligned LLMs has enabled a more powerful threat model in which attackers can now directly manipulate internal activations or weights to bypass refusal while preserving model utility, gaining fine-grained control over model behavior that prompt-level attacks may not achieve. Understanding these attacks is critical both for developing robust defenses and for illuminating the geometric structure of safety mechanisms in neural networks.

Therefore, there have been recent *representation-level* jailbreaking attacks that manipulate model latent space activations (Arditi et al., 2024; Li et al., 2025a; Schwinn et al., 2024). More specifically a current state-of-the-art representation attack, *Refusal Feature Ablation* (RFA) (Arditi et al., 2024), identifies a single “refusal direction” by computing the difference of means between harmful and harmless prompt activations, then applies orthogonal projections at every network layer to eliminate components along this direction. By using a very popular method, the difference-in-means vector as a direction to enable LLM generation control during inference (Turner et al., 2023; Li et al., 2023a; Rimsky et al., 2024), RFA has proven influential: it has enabled mechanistic analysis of jailbreaking (Jain et al., 2024), inspired robust adversarial training methods (Yu et al., 2025), and demonstrated the brittleness of current alignment techniques. However, RFA operates under a

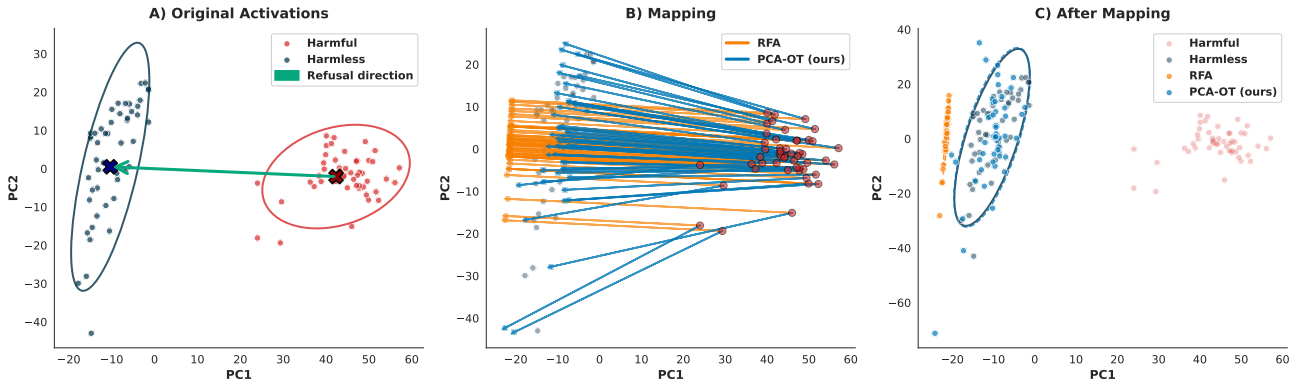


Figure 1. Two-dimensional PCA projections of harmful (red) and harmless (grey) activations at layer 28 of Qwen2.5-14B-Instruct. Left: original distributions with clear separation. Center: displacement vectors. Right: harmful activations after optimal transport. In contrast to RFA (Arditi et al., 2024), our OT-transformed harmful activations overlap harmless distribution while maintaining coherent structure.

restrictive assumption, that refusal can be characterized as variation along a single direction in activation space. This one-dimensional perspective ignores potential multi-dimensional and geometric structure in how models represent safety-relevant features and requires intervention across all layers to achieve effectiveness.

We propose a fundamentally different approach grounded in *optimal transport theory* (Santambrogio, 2015; Peyré & Cuturi, 2020). Rather than identifying and removing a refusal direction, we frame representation-level jailbreaking as a distribution-matching problem consisting in transforming the distribution of harmful activations  $\mu$  to match the distribution of harmless activations  $\nu$  via a minimal-cost mapping. Optimal transport provides a principled mathematical framework for this transformation, naturally capturing multi-dimensional covariance structure that projection-based methods ignore. For language model representations with thousands of dimensions, we combine this approach with principal component analysis to reduce computational complexity while preserving the essential geometric properties that distinguish harmful from harmless representations.

We introduce three main innovations:

- **Optimal transport for jailbreaking:** We provide the first application of Gaussian OT to representation-level jailbreaking, demonstrating that distributional matching outperforms directional removal (Sec. 2.1 and 2.2).
- **PCA-regularized transport:** To address the curse of dimensionality and prevent overfitting to noise, we combine OT with PCA, restricting transport to a low-dimensional subspace ( $r \ll d$ ) that captures essential distributional differences. We discuss a theoretical computational comparison (Sec. 2.4), indicating that our method is computationally comparable to the 1D methods.
- **Layer-selective intervention:** Through extensive

empirical analysis on six models spanning three families (Llama-2-7B/13B, Llama-3.1-8B, Qwen-2.5-7B/14B/32B), we find that applying OT to 1-2 carefully selected layers (40-60% of the network depth) yields superior attack success and text quality compared to a full-network intervention. This challenges prevailing assumptions about distributed refusal mechanisms and suggests localized intervention (Sec. 2.5).

## 2. Method

### 2.1. Problem Formulation

Consider a safety-aligned language model with last token (residual stream) activations at layer  $\ell$ , denoted  $\mathbf{h}_\ell \in \mathbb{R}^d$ , where  $d$  represents the model’s hidden dimension (typically ranging from 4096 to 8192 for modern language models). Given a dataset of harmful prompts that the model refuses to answer and harmless prompts that receive compliant responses, Arditi et al. (2024)’s objective is to transform the harmful activations to induce the model to comply with harmful requests.

Formally, let  $\mathcal{H}$  denote the set of harmful prompts and  $\mathcal{S}$  the set of harmless (safe) prompts. For each prompt  $p$ , we extract the activation at layer  $\ell$  and position  $\tau$  (typically the last token position), obtaining activation sets  $X_{\mathcal{H}}^{(\ell)} = \{\mathbf{x}_i^{(\ell)}\}_{i=1}^{n_h}$  and  $X_{\mathcal{S}}^{(\ell)} = \{\mathbf{x}_j^{(\ell)}\}_{j=1}^{n_s}$ , where  $\mathbf{x}_i^{(\ell)} \in \mathbb{R}^d$  represents the activation for the  $i$ -th harmful prompt at layer  $\ell$ .

RFA’s approach (Arditi et al., 2024) leverages the difference-in-means vector  $\mathbf{d} = \bar{\mathbf{x}}_{\mathcal{H}} - \bar{\mathbf{x}}_{\mathcal{S}}$  (Turner et al., 2023; Li et al., 2023a; Rimsky et al., 2024) and apply an orthogonal projection  $T_{\text{proj}}(\mathbf{x}) = (\mathbf{I} - \mathbf{P})\mathbf{x}$  where  $\mathbf{P} = \mathbf{d}\mathbf{d}^\top / \|\mathbf{d}\|^2$  is a rank-1 projection matrix. This removes the component of  $\mathbf{x}$  aligned with the mean difference direction via a rank-1 perturbation of the identity map. While computationally

simple and employed in prior work, this approach operates purely at the level of first-order statistics (means) and ignores the full distributional structure of the activation spaces. When viewing the activation sets as empirical probability distributions, this transformation is generally suboptimal. It does not account for variance, covariance structure, or higher-order distributional differences between harmful and harmless activations.

From an optimal transport perspective, our goal is to learn a transformation  $T^{(\ell)} : \mathbb{R}^d \rightarrow \mathbb{R}^d$  that pushes forward the empirical distribution of harmful activations to the empirical distribution of harmless activations.

## 2.2. Optimal Transport Framework

Given two probability measures  $\mu$  (harmful distribution) and  $\nu$  (harmless distribution) on  $\mathbb{R}^d$ , optimal transport seeks a mapping  $T$  that pushes forward  $\mu$  to  $\nu$  while minimizing the expected cost  $\mathbb{E}_{\mathbf{x} \sim \mu} [\|\mathbf{x} - T(\mathbf{x})\|^2]$  (Santambrogio, 2015; Peyré & Cuturi, 2020). When both distributions are Gaussian with means  $\mu_1, \mu_2$  and covariances  $\Sigma_1, \Sigma_2$ , the optimal transport map has the affine form:

$$T(\mathbf{x}) = \mathbf{A}\mathbf{x} + \mathbf{b}, \quad (1)$$

where the transport matrix  $\mathbf{A}$  and shift vector  $\mathbf{b}$  are given by the formulae:

$$\begin{aligned} \mathbf{A} &= \Sigma_1^{-1/2} (\Sigma_1^{1/2} \Sigma_2 \Sigma_1^{1/2})^{1/2} \Sigma_1^{-1/2}, \\ \mathbf{b} &= \mu_2 - \mathbf{A}\mu_1. \end{aligned} \quad (2)$$

This closed-form solution provides computational efficiency compared to iterative optimization approaches. The matrix  $\mathbf{A}$  captures how the covariance structure must be transformed, while the vector  $\mathbf{b}$  aligns the means.

To understand the relationship with prior work, consider the special case where  $\Sigma_1 = \Sigma_2 = \Sigma$ . In this setting, the transport matrix simplifies to  $\mathbf{A} = \mathbf{I}$ , yielding a pure translation  $T(\mathbf{x}) = \mathbf{x} + (\mu_2 - \mu_1)$ , which is used in Turner et al. (2023), and termed difference-in-means by Belrose (2023). Refusal Feature Ablation (RFA) (Arditi et al., 2024) takes a different approach: rather than translating activations along the difference-in-means direction  $\mathbf{d} = \mu_2 - \mu_1$ , it removes the component aligned with this direction via the orthogonal projection  $T_{\text{proj}}(\mathbf{x}; \mathbf{d}) = (\mathbf{I} - \mathbf{d}\mathbf{d}^\top / \|\mathbf{d}\|^2)\mathbf{x}$ . This works under the assumption that refusal happens along a 1D subspace and so suppressing it effectively destroys the model’s ability to tell apart harmful from harmless prompts. While both approaches operate at the level of first-order statistics when covariances are equal, neither accounts for potential differences in covariance structure between harmful and harmless distributions.

## 2.3. Dimensionality Reduction via PCA

Computing optimal transport maps in the full  $d$ -dimensional space faces two challenges. First, with sample sizes typically in the hundreds but dimensions in the thousands, empirical covariance estimates become ill-conditioned. Second, computing matrix square roots of high-dimensional matrices is computationally expensive and numerically unstable. To address these issues, we apply principal component analysis before computing the optimal transport map.

Given activation matrices  $\mathbf{X}_{\mathcal{H}} \in \mathbb{R}^{n_h \times d}$  and  $\mathbf{X}_{\mathcal{S}} \in \mathbb{R}^{n_s \times d}$ , we first compute a pooled mean:

$$\mu_{\text{pool}} = \frac{n_h \mu_{\mathcal{H}} + n_s \mu_{\mathcal{S}}}{n_{\mathcal{H}} + n_{\mathcal{S}}} \quad (3)$$

We then center both datasets using this pooled mean and compute the top  $k$  principal components from the combined centered data matrix  $\mathbf{Z} = [\mathbf{X}_{\mathcal{H}} - \mu_{\text{pool}}; \mathbf{X}_{\mathcal{S}} - \mu_{\text{pool}}]$ . The projection matrix  $\mathbf{P} \in \mathbb{R}^{d \times k}$  contains the top  $k$  right singular vectors of  $\mathbf{Z}$ .

Projecting to the  $k$ -dimensional subspace yields:

$$\mathbf{Y}_{\mathcal{H}} = (\mathbf{X}_{\mathcal{H}} - \mu_{\text{pool}})\mathbf{P}, \quad \mathbf{Y}_{\mathcal{S}} = (\mathbf{X}_{\mathcal{S}} - \mu_{\text{pool}})\mathbf{P}. \quad (4)$$

We then compute Gaussian optimal transport in this reduced  $k$ -dimensional space, obtaining  $\mathbf{A}_k \in \mathbb{R}^{k \times k}$  and  $\mathbf{b}_k \in \mathbb{R}^k$  using Eq. 2 (with empirical covariance matrices of projected data). To apply this transformation in the original space, we lift it back through the projection:

$$\mathbf{A}_{\text{full}} = \mathbf{P}\mathbf{A}_k\mathbf{P}^\top, \quad \mathbf{b}_{\text{full}} = \mu_2 - \mathbf{A}_{\text{full}}\mu_1 \quad (5)$$

where  $\mu_1$  and  $\mu_2$  are the means of  $\mathbf{X}_{\mathcal{H}}$  and  $\mathbf{X}_{\mathcal{S}}$  in the original space. The final transformation applied during model inference is:

$$T^{(\ell)}(\mathbf{x}) = \mathbf{A}_{\text{full}}\mathbf{x} + \mathbf{b}_{\text{full}}. \quad (6)$$

The choice of  $k$  involves a trade-off. Smaller values reduce overfitting and improve computational efficiency but may fail to capture important aspects of the distribution structure. Larger values preserve more information but risk overfitting to noise in the training activations.

## 2.4. Computational Considerations

The idea behind our PCA+OT strategy is that semantic shifts happen along low-dimensional subspaces of the representation space. Unlike previous works (Turner et al., 2023; Belrose, 2023; Arditi et al., 2024) which work along a one-dimensional subspace, our approach balances simplicity and efficacy (success rate of the attack) via a low-rank estimation of the optimal transport map via top- $k$  SVD.

**Algorithm 1** PCA-Gaussian Optimal Transport Jailbreaking

- 1: **Input:** Model  $f$ , harmful prompts  $\mathcal{H}$ , harmless prompts  $\mathcal{S}$ , components  $k$ , layers  $[\ell_{\text{start}}, \ell_{\text{end}}]$
- 2: **Training Phase:**
- 3: **for**  $\ell = \ell_{\text{start}}$  to  $\ell_{\text{end}}$  **do**
- 4:   Extract residual stream activations:  $\mathbf{X}_{\mathcal{H}}^{(\ell)}, \mathbf{X}_{\mathcal{S}}^{(\ell)}$
- 5:   Compute pooled mean  $\boldsymbol{\mu}_{\text{pool}}$
- 6:   Center:  $\mathbf{Z} = [\mathbf{X}_{\mathcal{H}}^{(\ell)} - \boldsymbol{\mu}_{\text{pool}}; \mathbf{X}_{\mathcal{S}}^{(\ell)} - \boldsymbol{\mu}_{\text{pool}}]$
- 7:   SVD:  $\mathbf{Z} = \mathbf{U}\boldsymbol{\Sigma}\mathbf{V}^\top$ , set  $\mathbf{P} = \mathbf{V}[:, :k]$
- 8:   Project:  $\mathbf{Y}_{\mathcal{H}} = (\mathbf{X}_{\mathcal{H}}^{(\ell)} - \boldsymbol{\mu}_{\text{pool}})\mathbf{P}$
- 9:      $\mathbf{Y}_{\mathcal{S}} = (\mathbf{X}_{\mathcal{S}}^{(\ell)} - \boldsymbol{\mu}_{\text{pool}})\mathbf{P}$
- 10:   Compute Gaussian OT:  $\mathbf{A}_k^{(\ell)}, \mathbf{b}_k^{(\ell)}$  from  $\mathbf{Y}_{\mathcal{H}}$  to  $\mathbf{Y}_{\mathcal{S}}^{(\ell)}$
- 11:   Lift:  $\mathbf{A}^{(\ell)} = \mathbf{P}\mathbf{A}_k^{(\ell)}\mathbf{P}^\top$
- 12:      $\mathbf{b}^{(\ell)} = \boldsymbol{\mu}_2^{(\ell)} - \mathbf{A}^{(\ell)}\boldsymbol{\mu}_1^{(\ell)}$
- 13: **end for**
- 14: **Inference Phase:**
- 15: Install hooks:  $\mathbf{h}_\ell \leftarrow \mathbf{A}^{(\ell)}\mathbf{h}_\ell + \mathbf{b}^{(\ell)}$  for  $\ell \in [\ell_{\text{start}}, \ell_{\text{end}}]$
- 16: **Return:** Modified model with transformations

Computing the top- $k$  SVD and the ensuing transport map (2) in the corresponding  $k$ -dimensional subspace has time complexity  $\tilde{O}(n_h dk + n_s k^2 + k^3)$ , where  $d$  is the dimensionality of the activations space. Once computed, the transport map can be applied at a computational cost of  $\tilde{O}(dk^2 + k^3)$  per token per layer. For moderate values of  $k$  (i.e.,  $k \ll \min(d, k)$ ), this computational cost is comparable to the 1D methods (Turner et al., 2023; Arditì et al., 2024), while leading to much higher attack success rates.

### 2.5. Layer-Selective Application and Algorithm

Algorithm 1 summarizes our complete approach. The method takes as input a language model, datasets of harmful and harmless prompts, the number of principal components  $k$ , and the intervention layer range  $[\ell_{\text{start}}, \ell_{\text{end}}]$ . During the training phase, we extract activations from the unmodified model for all prompts and compute independent optimal transport maps for each target layer. During inference, we apply these learned transformations as forward hooks on the specified layers. In contrast to prior work that applies interventions across all layers (Arditi et al., 2024; Rodríguez et al., 2025), our empirical analysis (Sec. 4.2 and 4.1) reveals that intervening at only 1-2 carefully validation-selected layers achieves optimal attack success while preserving model utility. This layer selectivity provides both computational efficiency and superior generation quality, as we demonstrate through systematic ablation studies.

## 3. Experimental Setup

This section describes the experimental setup, which is widely inspired from Arditì et al. (2024).

### 3.1. Models and Datasets

We evaluate our method across six models from two prominent language model families. From the Llama family (Touvron et al., 2023; Grattafiori et al., 2024), we test Llama-2-7B-chat, Llama-2-13B-chat, and Llama-3.1-8B-Instruct. From the Qwen family (Yang et al., 2024), we evaluate Qwen2.5-7B-Instruct, Qwen2.5-14B-Instruct, and Qwen2.5-32B-Instruct. These models span 7 to 32 billion parameters and represent diverse training methodologies and architectural choices, providing a robust testbed for evaluating attack generalization. Similar to Arditì et al. (2024), we use chat templates without system prompts.

For training our activation transformations, we adopt the dataset construction protocol from Arditì et al. (2024). The harmful dataset contains carefully curated examples of harmful requests across multiple risk categories, including chemical and biological weapons, cybercrime, harassment, misinformation, and illegal activities. This dataset aggregates samples from ADVBENCH (Zou et al., 2023b), MALICIOUSINSTRUCT (Huang et al., 2023), TDC2023 (Mazeika et al., 2023), and HARBENCH (Mazeika et al., 2024). The harmless dataset comprises instruction-following examples from ALPACA (Taori et al., 2023). Following (Arditi et al., 2024), we use 128 training samples for estimating parameters of transformation maps of Sec. 3.2 and 32 validation samples to tune their hyperparameters. We evaluate the success rate on the HARBENCH (Mazeika et al., 2024) test set, which is the same testing set as in Arditì et al. (2024).

### 3.2. Baseline Methods

We compare our method against two state-of-the-art approaches: one from representation-based jailbreaking and one from inference-time control of LLM generation. The first baseline, *refusal feature ablation* (RFA) (Arditi et al., 2024), computes the difference of means between harmful and harmless activations at each layer, then applies orthogonal projection to remove this direction across *all layers*. Following the recent paper work of Yu et al. (2025), the refusal direction is extracted from the last token activation.

The second baseline, AcT (Rodríguez et al., 2025), learns feature-wise linear optimal transport maps between source and target activation distributions. By treating each neuron independently, it estimates 1D transport maps using regression, providing an affine transformation per feature. Originally introduced for controlling toxicity, truthfulness, and diffusion model generation, we include it as a recent

state-of-the-art method in LLM generation control that is also inspired by optimal transport principles.

### 3.3. Evaluation Metrics

We measure attack success using a primary metric: LlamaGuard-2 (Team, 2024), a specialized safety classifier trained to detect harmful content in model outputs. We compute the attack success rate (ASR) as the fraction of test prompts for which LlamaGuard-2 judges the output as harmful, indicating successful jailbreaking. As a secondary metric, we employ substring matching against a curated list of refusal phrases from Ardit et al. (2024), though this metric can be circumvented by models that provide harmful content without explicit refusal language. To assess whether our transformations preserve model quality or utility, we measure perplexity (PPL) on two benchmark datasets. Pile perplexity evaluates general language modeling capability on a diverse corpus, while Alpaca perplexity measures instruction-following quality on user instructions paired with high-quality responses. Lower perplexity indicates that the generated text remains natural and consistent with the model’s learned language patterns.

## 4. Results and Discussion

This section presents the main results, ablation studies, and discussion our method and its limitations.

### 4.1. Main Results

Tab. 1 presents our primary results, with attack success rate and generation quality across methods and models.

**Single-Layer Intervention (PCA-OT<sub>1</sub>).** On the Llama family, our single-layer variant PCA-OT<sub>1</sub> consistently outperforms all baselines while maintaining excellent generation quality. PCA-OT<sub>1</sub> achieves 77.12% ASR on Llama-2-7B (versus 74.95% for AcT), 79.25% on Llama-2-13B (versus 78.51% for AcT), and 74.69% on Llama-3.1-8B (versus 74.32% for AcT). Critically, these improvements come with superior model utility as measured by perplexity: on Llama-2-13B, PCA-OT<sub>1</sub> achieves 8.41 Pile perplexity compared to AcT’s 11.16, while maintaining perplexity comparable to both RFA and the unmodified baseline. This demonstrates that single-layer PCA-Gaussian OT effectively targets refusal mechanisms without degrading general language modeling capabilities, outperforming RFA despite intervening at only one layer versus RFA’s all-layer intervention.

On the Qwen family, however, PCA-OT<sub>1</sub> exhibits inconsistent performance relative to RFA: it achieves marginal improvement on Qwen2.5-7B (79.40% versus 77.94%), but underperforms on Qwen2.5-14B (69.81% versus 79.45%). This architectural dependence suggests that Qwen’s safety mechanisms may be distributed differently than Llama’s,

potentially requiring intervention at multiple network depths to fully bypass alignment. These observations motivated our two-layer variant.

**Two-Layer Intervention (PCA-OT<sub>2</sub>).** On the Qwen family (also Llama family), PCA-OT<sub>2</sub> decisively surpasses RFA: 81.76% on Qwen2.5-7B (+3.8pp), 83.81% on Qwen2.5-14B (+4.4pp), and 75.94% on Qwen2.5-32B (+18.3pp). However, this increased effectiveness may come with generation quality tradeoffs on some models. On Qwen2.5-7B, Pile perplexity increases to 10.56 compared to RFA’s 7.94, while Alpaca perplexity rises to 24.66. Similarly, on Llama-2-7B, perplexity increases to 15.93 compared to the baseline’s 9.21. However, on Llama-2-13B and Qwen2.5-14B, PCA-OT<sub>2</sub> maintains reasonable perplexity (9.40 and 7.54, respectively), indicating that the optimal number of intervention layers may be model-dependent.

**Comparison to AcT.** Across all model families, PCA-OT<sub>1</sub> consistently outperforms AcT on attack success while maintaining comparable or better perplexity. Improvements range from +2.17pp on Llama-2-7B to +10.58pp on Qwen2.5-32B, with perplexity advantages particularly pronounced on Llama models. This demonstrates that accounting for cross-dimensional dependencies through optimal transport yields more effective refusal ablation than independent per-dimension transformations.

**Sanity Check: Layer-Matched Baseline Comparison.** Before analyzing the hyperparameters of our PCA-OT method, we first verify that our improvements stem from optimal transport rather than merely advantageous layer selection. To isolate these effects, we conduct a controlled sanity check by evaluating all methods at the same intervention layers—specifically, the layers where each baseline performs optimally. We consider two configurations on Llama-2-13B-chat-hf: (1) layers optimized for RFA (layer 24 for direction extraction, with RFA still projecting across all layers during inference), and (2) layer optimized for AcT (layer 22). These represent the layer selections that produced the baseline results in Tab. 1. For each configuration, we run PCA-OT<sub>1</sub> at the same intervention layers as the corresponding baseline, ensuring a fair comparison where layer selection advantages are neutralized.

Tab. 2 presents the results. In both configurations, PCA-OT achieves the highest ASR. When evaluated at RFA’s optimal layer or AcT’s optimal layer, with comparable perplexity to RFA, and lower than AcT. This validates that PCA-OT’s superiority is not an artifact of layer selection.

Additional results are presented in App. A.2, including a sanity check evaluations on complex reasoning benchmarks (Tab. 9), which demonstrate that our intervention method preserves general capabilities, achieving performance comparable to the unmodified baseline across MMLU, Truth-

Table 1. Attack success rate and generation quality across methods and models (mean  $\pm$  standard error over 4 seeds). Our PCA-Gaussian OT method consistently achieves the highest attack success rates. Best ASR per model is **bolded**; second-best is underlined.

Model	Method	LlamaGuard ASR (%)	Pile PPL	Alpaca PPL
<i>Llama-2-7b-chat-hf (32 layers)</i>				
	Baseline (no intervention)	0.62	9.21	4.99
	RFA	70.65 $\pm$ 0.53	9.16 $\pm$ 0.00	4.89 $\pm$ 0.00
	AcT	74.95 $\pm$ 1.00	10.54 $\pm$ 0.80	4.91 $\pm$ 0.14
	PCA-OT <sub>1</sub> (ours)	77.12 $\pm$ 1.63	9.36 $\pm$ 0.05	4.74 $\pm$ 0.01
	PCA-OT <sub>2</sub> (ours)	<b>80.42 <math>\pm</math> 0.32</b>	15.93 $\pm$ 1.22	6.22 $\pm$ 0.30
<i>Llama-2-13b-chat-hf (40 layers)</i>				
	Baseline (no intervention)	1.26	8.01	4.97
	RFA	46.49 $\pm$ 1.64	8.04 $\pm$ 0.00	4.86 $\pm$ 0.01
	AcT	78.51 $\pm$ 1.75	11.16 $\pm$ 0.70	5.32 $\pm$ 0.17
	PCA-OT <sub>1</sub> (ours)	79.25 $\pm$ 1.64	8.41 $\pm$ 0.02	4.76 $\pm$ 0.01
	PCA-OT <sub>2</sub> (ours)	<b>83.81 <math>\pm</math> 0.16</b>	9.40 $\pm$ 0.13	4.90 $\pm$ 0.04
<i>Llama-3.1-8B-Instruct (32 layers)</i>				
	Baseline (no intervention)	1.64	8.68	6.01
	RFA	72.69 $\pm$ 1.05	8.75 $\pm$ 0.00	6.05 $\pm$ 0.01
	AcT	74.32 $\pm$ 1.11	10.65 $\pm$ 0.47	7.31 $\pm$ 0.24
	PCA-OT <sub>1</sub> (ours)	74.69 $\pm$ 1.42	9.18 $\pm$ 0.02	6.41 $\pm$ 0.01
	PCA-OT <sub>2</sub> (ours)	<b>83.49 <math>\pm</math> 0.47</b>	10.61 $\pm$ 0.14	7.51 $\pm$ 0.09
<i>Qwen2.5-7B-Instruct (28 layers)</i>				
	Baseline (no intervention)	8.17	7.55	6.12
	RFA	77.94 $\pm$ 0.34	7.94 $\pm$ 0.02	6.51 $\pm$ 0.02
	AcT	75.05 $\pm$ 1.14	7.85 $\pm$ 0.04	6.76 $\pm$ 0.09
	PCA-OT <sub>1</sub> (ours)	79.40 $\pm$ 0.16	9.40 $\pm$ 0.29	12.92 $\pm$ 2.00
	PCA-OT <sub>2</sub> (ours)	<b>81.76 <math>\pm</math> 0.93</b>	10.56 $\pm$ 2.23	24.66 $\pm$ 17.61
<i>Qwen2.5-14B-Instruct (48 layers)</i>				
	Baseline (no intervention)	3.14	6.63	6.29
	RFA	79.45 $\pm$ 0.88	6.72 $\pm$ 0.02	6.44 $\pm$ 0.03
	AcT	59.96 $\pm$ 2.98	7.02 $\pm$ 0.05	5.82 $\pm$ 0.09
	PCA-OT <sub>1</sub> (ours)	84.43 $\pm$ 3.45	8.16 $\pm$ 0.30	8.07 $\pm$ 0.65
	PCA-OT <sub>2</sub> (ours)	<b>83.81 <math>\pm</math> 0.16</b>	7.54 $\pm$ 0.07	6.37 $\pm$ 0.12
<i>Qwen2.5-32B-Instruct (64 layers)</i>				
	Baseline (no intervention)	8.80	6.41	5.59
	RFA	57.55 $\pm$ 2.08	6.44 $\pm$ 0.01	5.76 $\pm$ 0.03
	AcT	35.17 $\pm$ 2.73	6.49 $\pm$ 0.01	5.95 $\pm$ 0.04
	PCA-OT <sub>1</sub> (ours)	45.75 $\pm$ 2.12	6.55 $\pm$ 0.00	6.29 $\pm$ 0.04
	PCA-OT <sub>2</sub> (ours)	<b>75.94 <math>\pm</math> 0.47</b>	6.99 $\pm$ 0.02	7.45 $\pm$ 0.12

Table 2. Layer-matched comparison on Llama-2-13B-chat-hf at baseline-optimal layers. PCA-OT achieves highest attack success regardless of layer selection strategy.

Method	Layer	LlamaGuard ASR (%)	Pile PPL
<i>Evaluated at RFA-optimal layer’s direction (24)</i>			
RFA	24	46.5	8.06
AcT	24	71.1	10.07
PCA-OT (ours)	24	<b>75.5</b>	8.95
<i>Evaluated at AcT-optimal layers (22)</i>			
RFA	22	26.4	8.13
AcT	22	77.4	10.62
PCA-OT (ours)	22	<b>78.6</b>	8.84

fulQA, ARC-Challenge, and GSM8K.

## 4.2. Ablation Studies

We conduct a comprehensive investigation into the sensitivity of the interventional layer and the role of the number of principal components.

**Interventional Layer Sensitivity.** Tab. 3 and Fig. 4 present attack success rate and perplexity as functions of network depth for both Llama-2-13b and Qwen2.5-14B.

For Llama-2-13B, ASR shows a sharp transition at 35-45 % depth, jumping from 34.0% (layer 11) to 82.4% (layer 17), then plateauing at 72-82% through layer 38. Optimal attacks (layer 17) cause modest perplexity degradation (8.59 vs. 8.01 baseline), while extreme depths severely impact quality (14.90 at 95% depth). Qwen2.5-14B exhibits a gradual transition, with ASR increasing from 2.5% (layer 6) to 66.7% (layer 30), then declining to 23.3% at layer

Table 3. Layer sensitivity analysis for PCA-Gaussian OT with  $k=2$  components. Llama-2-13B exhibits a sharp transition to high ASR at 40–50% depth, while Qwen2.5-14B shows gradual increase peaking at 62.5% depth. Complete results in Appendix, Tab. 5.

MODEL	PEAK LAYER	ASR (%)	DEPTH (%)
LLAMA-2-13B	17	<b>82.4</b>	42.5
QWEN2.5-14B	30	<b>66.7</b>	62.5

Table 4. Component sensitivity analysis for PCA-Gaussian OT on Llama-2-13B-chat-hf. Optimal performance is achieved with  $K = 2$  components, balancing attack success with preservation of generation quality.

$K$	LlamaGuard ASR (%)	Substring ASR (%)	Pile PPL
1	81.1	95.0	<b>8.50</b>
2	<b>82.4</b>	94.3	8.59
5	80.5	<b>98.7</b>	12.2
10	76.1	<b>100.0</b>	45.1

45—a pattern absent in Llama. This suggests Qwen’s safety alignment is more distributed at deeper layers.

Overall, the results reveal a striking non-monotonic relationship: interventions at shallow layers (depth  $\leq 30\%$ ) fail to induce harmful completions (ASR  $< 5\%$ ), while middle layers (40–60% depth) achieve peak effectiveness, suggesting that refusal behavior crystallizes in a localized geometric structure within the middle layers. This is consistent with very recent findings on the representation quality in LLMs (Skean et al., 2025).

We finally show in Tab. 13 representative generations from Llama-2-13B with PCA-OT<sub>1</sub> at different, intervention depths. Optimal layers (L17) produce coherent harmful content, while deep layers (L32) exhibit pathological repetition despite high ASR.

**Role of the Number of Components  $K$ .** Recall from Sec. 2.3 that PCA enables accurate dimensionality reduction prior to optimal transport, addressing the ill-conditioned covariance problem that arises when sample size (hundreds) is substantially smaller than dimensionality (thousands). Fig. 2 presents the individual and cumulative explained variance for harmful and harmless activations. The first few principal components capture substantial variance: the top three components alone explain  $\geq 40\%$  of variance in both Llama-2-13B and Qwen2.5-14B. Fig. 3 shows the cosine similarity between mapped harmful and harmless activations as a function of  $K$ . As expected, increasing  $K$  improves covariance estimation accuracy, reflected in higher similarity scores. However, empirical evaluation from Tabs. 4 and 6 reveals that optimal ASR is achieved at lower values of  $K$  for both Llama-2-13B and Qwen2.5-14B. This confirms the theoretical intuition from Sec. 2.3: while larger  $K$  yields more accurate statistical estimation, it also increases vulnerability to noise, creating a bias-variance tradeoff where moderate dimensionality reduction proves most effective.

### 4.3. Geometric Interpretation and Computational Time

To provide geometric intuition for PCA-OT’s effectiveness, we visualize activation distributions in PCA space. Fig. 1 shows two-dimensional projections of harmful and harmless activations before (left) and after transformation (right), along with displacement vectors for our method and RFA (Arditi et al., 2024). The harmful cluster exhibits larger variance than the harmless cluster, particularly along the first principal component. RFA (Arditi et al., 2024) produces transformed distributions imperfectly aligned with the harmless target. As shown in the right panel, RFA’s transformation collapses variance along the first principal component, while the harmless distribution does not. In contrast, our PCA-OT produces transformed distributions that closely match the harmless cluster in both mean and covariance structure, explaining its superior attack-quality tradeoff. Computational time is discussed in App. A.1.2.

### 4.4. Limitations and Future Work

Our largest tested model, Qwen2.5-32B, proves substantially more resistant to all attacks (75.9% ASR vs. 80–84% on smaller models), suggesting that scale may provide genuine robustness through more distributed safety mechanisms. Furthermore, our evaluation does not include recent defense methods such as RepNoise (Rosati et al., 2024), latent adversarial training (Yu et al., 2025), or Vaccine (Huang et al., 2024). Comprehensive evaluation against these defenses would strengthen understanding of the attack-defense landscape and reveal whether distributional transport attacks remain effective against adversarially-trained models.

We extract activations at the last token position, as this contains the model’s final representation before generation. However, alternative strategies such as mean pooling across sequence positions or attention-weighted pooling could potentially reduce overfitting to positional noise. Additionally, our method assumes approximately Gaussian activation distributions. While visualizations show Gaussianity, extending to non-Gaussian settings through neural optimal transport could handle more complex activation geometries at increased computational cost.

## 5. Related Work

### 5.1. Safety Alignment and its Vulnerabilities

Modern language model alignment relies primarily on Reinforcement Learning from Human Feedback (RLHF) (Ouyang et al., 2022; Bai et al., 2022), which trains a reward model on human preference judgments and optimizes the policy via proximal policy optimization. Direct preference optimization (DPO) (Rafailov et al., 2023) and variants (Azar et al., 2024; Ethayarajh et al., 2024; Meng et al., 2024) eliminate the explicit reward model by deriving

a closed-form mapping from reward functions to optimal policies, enabling alignment through a single maximum likelihood objective. However, [Sharma et al. \(2024\)](#) demonstrate that safety alignment affects the first few output tokens, explaining vulnerabilities to suffix attacks ([Zou et al., 2023b](#)), prefilling attacks ([Li et al., 2025b](#)), and fine-tuning attacks ([Zhan et al., 2024](#)).

Fine-tuning attacks expose alignment fragility. More specifically, [Lermen & Rogers-Smith \(2024\)](#) show that even benign fine-tuning degrades safety guardrails, while [Zhan et al. \(2024\)](#) achieves aims to achieve the removal of RLHF protections via targeted fine-tuning. These findings indicate that alignment induces brittle distributional changes rather than robust behavioral constraints. In contrast to these parameter-modification approaches that require model access, leave permanent traces, and require prompt instructions and completions, our optimal transport framework operates entirely at inference time by computing geometric transformations in activation space, enabling black-box attacks that preserve model parameters, and only need prompt instructions.

## 5.2. Adversarial Attacks on Language Models

Adversarial attacks on LLMs span discrete token optimization, continuous latent manipulation, and representation-level interventions. The Greedy Coordinate Gradient (GCG) attack ([Zou et al., 2023b](#)) pioneered optimization-based jailbreaking by finding universal adversarial suffixes that transfer across models. Subsequent work has substantially improved efficiency and success rates ([Li et al., 2024a](#); [Liao & Sun, 2024](#); [Andriushchenko et al., 2025](#)).

Semantic jailbreaking methods generate human-readable attacks that evade perplexity-based detection. AutoDAN ([Liu et al., 2024](#)) employs hierarchical genetic algorithms to evolve semantically meaningful prompts, and role-playing attacks ([Shah et al., 2023](#)) embed harmful requests in fictional scenarios, while multi-step jailbreaking ([Mehrotra et al., 2024](#)) decomposes harmful objectives into benign sub-tasks that individually pass safety filters. Unlike these discrete token optimization and prompt-specific methods with limited transferability, representation-level attacks manipulate continuous activation distributions, providing a more general and principled approach to understanding and exploiting alignment vulnerabilities.

[Arditi et al. \(2024\)](#) is a pioneering work in representation-based jailbreaking, and directly inspires our approach. However, while they build a mapping in activation space through the difference-in-means direction, our work employs optimal transport to compute geometrically principled transport maps between harmful and harmless activation distributions, providing a more theoretically grounded framework for understanding and reversing alignment via representations.

## 5.3. Inference-Time Generation Control and OT for Robustness and LLM

Inference-time control methods manipulate token distributions without modifying parameters. Contrastive Decoding ([Li et al., 2023b](#)) maximizes weighted log-likelihood differences between expert and amateur models. Representation Engineering ([Zou et al., 2023a](#)) introduces steering vectors that modify residual stream activations.

Optimal transport provides a mathematically principled framework for comparing and transforming probability distributions. AcT ([Rodriguez et al., 2025](#)) applies optimal transport (OT) for activation steering, with applications on the control of toxicity, truthfulness, and diffusion model generation. Although inspired by optimal transport, AcT applies a 1D affine feature transformation, which is distinct from our method. Our method directly uses multidimensional Gaussian OT, and is the first work in jailbreaking that uses OT. We include AcT as a state-of-the-art method for LLM generation control.

There have been works that study adversarial robustness through the lens of optimal transport. For example, [Bhagoji et al. \(2019\)](#) establish that the minimum transportation cost between class distributions yields a fundamental lower bound on adversarial robustness, thereby proving that optimal transport is the theoretically correct framework for characterizing adversarial perturbation limits. Recent work establishes connections between optimal transport and language models. GiLOT ([Li et al., 2024b](#)) uses optimal transport to measure distributional changes across vocabulary for feature attribution in LLMs. Alignment via optimal transport (AOT) ([Melnyk et al., 2024](#)) applies one-dimensional optimal transport to align distributional preferences, inducing stochastic dominance of the chosen over the rejected reward distributions. Still, to our knowledge, no prior work has applied optimal transport to adversarial attacks on language models. While optimal transport has been used for image adversarial examples and for LLM alignment, the intersection of optimal transport theory with LLM adversarial robustness remains unexplored. Our work addresses this gap by formulating adversarial attacks as distributional transport problems, leveraging optimal transport’s geometric structure to find minimal perturbations in representation space that induce jailbreaking behavior.

## 6. Conclusion

We introduced a principled framework for jailbreaking safety-aligned language models through optimal transport theory, demonstrating that viewing refusal ablation as a distributional matching problem yields substantial improvements over projection-based methods. By combining PCA-based dimensionality reduction with closed-form Gaussian

optimal transport, we achieve substantial higher attack success than state-of-the-art representation-level jailbreaking methods while often maintaining generation quality. Key insights emerge from our work. First, optimal transport provides genuine advantages over directional removal by jointly transforming both location and covariance structure of activation distributions, capturing multi-dimensional geometric patterns that simple projections miss. Second, refusal mechanisms localize to specific network depths (40-60%), with interventions at tuned layers achieving high attack success while preserving linguistic coherence. Finally, open questions include how to extend beyond Gaussian assumptions to handle complex activation geometries, and what defensive architectural modifications can break our distributional assumptions. By providing a mathematically principled framework for understanding representation-level jailbreaking, we hope to accelerate the development of more robust and trustworthy language models.

## Impact Statement

This paper presents research on adversarial attacks against safety-aligned language models. While such work has dual-use potential, we believe transparency about model vulnerabilities is essential for developing more robust safety mechanisms. Our method explicitly demonstrates weaknesses in current alignment approaches, providing concrete evidence that safety behaviors can be systematically reversed through principled manipulation of internal representations.

The primary societal benefit of this work lies in improving our understanding of adversarial robustness in language models, enabling development of more secure systems. By revealing how optimal transport can exploit distributional patterns in activations, we provide defenders with specific targets for hardening.

Potential negative impacts include misuse by malicious actors to bypass safety mechanisms in deployed systems. However, we note that similar attacks already exist in the literature, and our contribution primarily improves understanding rather than enabling entirely new threat vectors. Furthermore, responsible disclosure practices ensure that model developers are aware of these vulnerabilities and can take appropriate defensive measures.

## References

- Andriushchenko, M., Croce, F., and Flammarion, N. Jailbreaking leading safety-aligned llms with simple adaptive attacks. In *The Thirteenth International Conference on Learning Representations*, 2025.
- Arditi, A., Obeso, O., Syed, A., Paleka, D., Panickssery, N., Gurnee, W., and Nanda, N. Refusal in language models is mediated by a single direction. *Advances in Neural Information Processing Systems*, 37:136037–136083, 2024.
- Azar, M. G., Guo, Z. D., Piot, B., Munos, R., Rowland, M., Valko, M., and Calandriello, D. A general theoretical paradigm to understand learning from human preferences. In *International Conference on Artificial Intelligence and Statistics*, pp. 4447–4455. PMLR, 2024.
- Bai, Y., Jones, A., Ndousse, K., Askell, A., Chen, A., Das-Sarma, N., Drain, D., Fort, S., Ganguli, D., Henighan, T., et al. Training a helpful and harmless assistant with reinforcement learning from human feedback. *arXiv preprint arXiv:2204.05862*, 2022.
- Belrose, N. Diff-in-means concept editing is worst-case optimal: Explaining a result by Sam Marks and Max Tegmark. Blog post, EleutherAI, 2023. URL <https://blog.eleuther.ai/diff-in-means/>.
- Bhagoji, A. N., Cullina, D., and Mittal, P. Lower bounds on

- adversarial robustness from optimal transport. *Advances in Neural Information Processing Systems*, 32, 2019.
- Brown, T., Mann, B., Ryder, N., Subbiah, M., Kaplan, J. D., Dhariwal, P., Neelakantan, A., Shyam, P., Sastry, G., Askell, A., et al. Language models are few-shot learners. *Advances in neural information processing systems*, 33: 1877–1901, 2020.
- Chowdhery, A., Narang, S., Devlin, J., Bosma, M., Mishra, G., Roberts, A., Barham, P., Chung, H. W., Sutton, C., Gehrmann, S., et al. Palm: Scaling language modeling with pathways. *Journal of Machine Learning Research*, 24(240):1–113, 2023.
- Clark, P., Cowhey, I., Etzioni, O., Khot, T., Sabharwal, A., Schoenick, C., and Tafjord, O. Think you have solved question answering? try arc, the ai2 reasoning challenge. *arXiv preprint arXiv:1803.05457*, 2018.
- Cobbe, K., Kosaraju, V., Bavarian, M., Chen, M., Jun, H., Kaiser, L., Plappert, M., Tworek, J., Hilton, J., Nakano, R., et al. Training verifiers to solve math word problems. *arXiv preprint arXiv:2110.14168*, 2021.
- Dunefsky, J. and Cohan, A. One-shot optimized steering vectors mediate safety-relevant behaviors in llms. In *Second Conference on Language Modeling*, 2025.
- Ethayarajh, K., Xu, W., Muennighoff, N., Jurafsky, D., and Kiela, D. Kto: Model alignment as prospect theoretic optimization. *arXiv preprint arXiv:2402.01306*, 2024.
- Grattafiori, A., Dubey, A., Jauhri, A., Pandey, A., Kadian, A., Al-Dahle, A., Letman, A., Mathur, A., Schelten, A., Vaughan, A., et al. The llama 3 herd of models. *arXiv preprint arXiv:2407.21783*, 2024.
- Hendrycks, D., Basart, S., Kadavath, S., Mazeika, M., Arora, A., Guo, E., Burns, C., Puranik, S., He, H., Song, D., et al. Measuring coding challenge competence with apps. *arXiv preprint arXiv:2105.09938*, 2021.
- Huang, T., Hu, S., and Liu, L. Vaccine: Perturbation-aware alignment for large language models against harmful fine-tuning attack. *Advances in Neural Information Processing Systems*, 37:74058–74088, 2024.
- Huang, Y., Gupta, S., Xia, M., Li, K., and Chen, D. Catastrophic jailbreak of open-source llms via exploiting generation. *arXiv preprint arXiv:2310.06987*, 2023.
- Jain, S., Lubana, E. S., Oksuz, K., Joy, T., Torr, P., Sanyal, A., and Dokania, P. What makes and breaks safety fine-tuning? a mechanistic study. *Advances in Neural Information Processing Systems*, 37:93406–93478, 2024.
- Lermen, S. and Rogers-Smith, C. Lora fine-tuning efficiently undoes safety training in llama 2-chat 70b. In *ICLR 2024 Workshop on Secure and Trustworthy Large Language Models*, 2024.
- Li, K., Patel, O., Viégas, F., Pfister, H., and Wattenberg, M. Inference-time intervention: Eliciting truthful answers from a language model. *Advances in Neural Information Processing Systems*, 36:41451–41530, 2023a.
- Li, Q., Guo, Y., Zuo, W., and Chen, H. Improved generation of adversarial examples against safety-aligned llms. *Advances in Neural Information Processing Systems*, 2024a.
- Li, R., Wang, H., and Mao, C. Largo: Latent adversarial reflection through gradient optimization for jailbreaking llms. *arXiv preprint arXiv:2505.10838*, 2025a.
- Li, X., Chen, J., Chai, Y., and Xiong, H. Gilot: Interpreting generative language models via optimal transport. In *Forty-first International Conference on Machine Learning*, 2024b.
- Li, X. L., Holtzman, A., Fried, D., Liang, P., Eisner, J., Hashimoto, T. B., Zettlemoyer, L., and Lewis, M. Contrastive decoding: Open-ended text generation as optimization. In *Proceedings of the 61st annual meeting of the association for computational linguistics (volume 1: Long papers)*, pp. 12286–12312, 2023b.
- Li, Y., Hu, J., Sang, W., Ma, L., Xie, J., Zhang, W., Yu, A., Zhao, S., Huang, Q., and Zhou, Q. Prefill-based jailbreak: A novel approach of bypassing llm safety boundary. *arXiv preprint arXiv:2504.21038*, 2025b.
- Liao, Z. and Sun, H. Amplegcg: Learning a universal and transferable generative model of adversarial suffixes for jailbreaking both open and closed llms. In *First Conference on Language Modeling*, 2024.
- Lin, S., Hilton, J., and Evans, O. Truthfulqa: Measuring how models mimic human falsehoods. In *Proceedings of the 60th annual meeting of the association for computational linguistics (volume 1: long papers)*, pp. 3214–3252, 2022.
- Liu, X., Xu, N., Chen, M., and Xiao, C. Autodan: Generating stealthy jailbreak prompts on aligned large language models. In *The Twelfth International Conference on Learning Representations*, 2024.
- Mazeika, M., Hendrycks, D., Li, H., Xu, X., Hough, S., Zou, A., Rajabi, A., Yao, Q., Wang, Z., Tian, J., et al. The trojan detection challenge. In *NeurIPS 2022 Competition Track*, pp. 279–291. PMLR, 2023.
- Mazeika, M., Phan, L., Yin, X., Zou, A., Wang, Z., Mu, N., Sakhaee, E., Li, N., Basart, S., Li, B., et al. Harmbench:

- A standardized evaluation framework for automated red teaming and robust refusal. In *International Conference on Machine Learning*, pp. 35181–35224. PMLR, 2024.
- Mehrotra, A., Zampetakis, M., Kassianik, P., Nelson, B., Anderson, H., Singer, Y., and Karbasi, A. Tree of attacks: Jailbreaking black-box llms automatically. *Advances in Neural Information Processing Systems*, 37:61065–61105, 2024.
- Melnyk, I., Mroueh, Y., Belgodere, B., Rigotti, M., Nitsure, A., Yurochkin, M., Greenewald, K., Navratil, J., and Ross, J. Distributional preference alignment of llms via optimal transport. *Advances in Neural Information Processing Systems*, 37:104412–104442, 2024.
- Meng, Y., Xia, M., and Chen, D. Simpo: Simple preference optimization with a reference-free reward. In *Advances in Neural Information Processing Systems (NeurIPS)*, 2024.
- Ouyang, L., Wu, J., Jiang, X., Almeida, D., Wainwright, C., Mishkin, P., Zhang, C., Agarwal, S., Slama, K., Ray, A., et al. Training language models to follow instructions with human feedback. *Advances in neural information processing systems*, 35:27730–27744, 2022.
- Peyré, G. and Cuturi, M. Computational optimal transport, 2020. URL <https://arxiv.org/abs/1803.00567>.
- Rafailov, R., Sharma, A., Mitchell, E., Manning, C. D., Ermon, S., and Finn, C. Direct preference optimization: Your language model is secretly a reward model. *Advances in neural information processing systems*, 36:53728–53741, 2023.
- Rimsky, N., Gabrieli, N., Schulz, J., Tong, M., Hubinger, E., and Turner, A. Steering llama 2 via contrastive activation addition. In *Proceedings of the 62nd Annual Meeting of the Association for Computational Linguistics (Volume 1: Long Papers)*, pp. 15504–15522, 2024.
- Rodriguez, P., Blaas, A., Klein, M., Zappella, L., Apostoloff, N., Suau, X., et al. Controlling language and diffusion models by transporting activations. In *The Thirteenth International Conference on Learning Representations*, 2025.
- Rosati, D., Wehner, J., Williams, K., Bartoszcze, L., Gonzales, R., Majumdar, S., Sajjad, H., Rudzicz, F., et al. Representation noising: A defence mechanism against harmful finetuning. *Advances in Neural Information Processing Systems*, 37:12636–12676, 2024.
- Santambrogio, F. Optimal transport for applied mathematicians. *Progress in Nonlinear Differential Equations and Their Applications*, 2015.
- Schwinn, L., Dobre, D., Xhonneux, S., Gidel, G., and Günnemann, S. Soft prompt threats: Attacking safety alignment and unlearning in open-source llms through the embedding space. *Advances in Neural Information Processing Systems*, 37:9086–9116, 2024.
- Shah, R., Pour, S., Tagade, A., Casper, S., Rando, J., et al. Scalable and transferable black-box jailbreaks for language models via persona modulation. *arXiv preprint arXiv:2311.03348*, 2023.
- Sharma, M., Tong, M., Korbak, T., Duvenaud, D., Askell, A., Bowman, S. R., DURMUS, E., Hatfield-Dodds, Z., Johnston, S. R., Kravec, S. M., et al. Towards understanding sycophancy in language models. In *The Twelfth International Conference on Learning Representations*, 2024.
- Skean, O., Arefin, M. R., Zhao, D., Patel, N. N., Naghiyev, J., LeCun, Y., and Shwartz-Ziv, R. Layer by layer: Uncovering hidden representations in language models. In *Forty-second International Conference on Machine Learning*, 2025.
- Taori, R., Gulrajani, I., Zhang, T., Dubois, Y., Li, X., Guestrin, C., Liang, P., and Hashimoto, T. B. Stanford alpaca: An instruction-following llama model, 2023.
- Team, L. Meta llama guard 2. [https://github.com/meta-llama/PurpleLlama/blob/main/Llama-Guard2/MODEL\\_CARD.md](https://github.com/meta-llama/PurpleLlama/blob/main/Llama-Guard2/MODEL_CARD.md), 2024.
- Touvron, H., Martin, L., Stone, K., Albert, P., Almahairi, A., Babaei, Y., Bashlykov, N., Batra, S., Bhargava, P., Bhosale, S., et al. Llama 2: Open foundation and finetuned chat models. *arXiv preprint arXiv:2307.09288*, 2023.
- Turner, A. M., Thiergart, L., Leech, G., Udell, D., Vazquez, J. J., Mini, U., and MacDiarmid, M. Steering language models with activation engineering. *arXiv preprint arXiv:2308.10248*, 2023.
- Wu, J., Xie, Y., Yang, Z., Wu, J., Gao, J., Ding, B., Wang, X., and He, X. beta-dpo: Direct preference optimization with dynamic beta. *Advances in Neural Information Processing Systems*, 37:129944–129966, 2024.
- Yang, A., Yang, B., Zhang, B., Hui, B., Zheng, B., Yu, B., Li, C., Liu, D., Huang, F., Wei, H., Lin, H., Yang, J., Tu, J., Zhang, J., Yang, J., Yang, J., Zhou, J., Lin, J., Dang, K., Lu, K., Bao, K., Yang, K., Yu, L., Li, M., Xue, M., Zhang, P., Zhu, Q., Men, R., Lin, R., Li, T., Xia, T., Ren, X., Ren, X., Fan, Y., Su, Y., Zhang, Y., Wan, Y., Liu, Y., Cui, Z., Zhang, Z., and Qiu, Z. Qwen2.5 technical report. *arXiv preprint arXiv:2412.15115*, 2024.

- Yu, L., Do, V., Hambardzumyan, K., and Cancedda, N. Robust llm safeguarding via refusal feature adversarial training. In *The Thirteenth International Conference on Learning Representations*, 2025.
- Zhan, Q., Fang, R., Bindu, R., Gupta, A., Hashimoto, T. B., and Kang, D. Removing rlhf protections in gpt-4 via fine-tuning. In *Proceedings of the 2024 Conference of the North American Chapter of the Association for Computational Linguistics: Human Language Technologies (Volume 2: Short Papers)*, pp. 681–687, 2024.
- Zou, A., Phan, L., Chen, S., Campbell, J., Guo, P., Ren, R., Pan, A., Yin, X., Mazeika, M., Dombrowski, A.-K., et al. Representation engineering: A top-down approach to ai transparency. *arXiv preprint arXiv:2310.01405*, 2023a.
- Zou, A., Wang, Z., Carlini, N., Nasr, M., Kolter, J. Z., and Fredrikson, M. Universal and transferable adversarial attacks on aligned language models. *arXiv preprint arXiv:2307.15043*, 2023b.

**Efficient Refusal Ablation in LLM through Optimal Transport**

Table 5. Layer sensitivity analysis for PCA-Gaussian OT with  $k = 2$  components across two model families. Llama-2-13B exhibits sharp transition to high ASR at 40–50% depth, while Qwen2.5-14B shows a gradual increase peaking at 62.5% depth, followed by a decline.

<b>LLAMA-2-13B-CHAT-HF (40 LAYERS)</b>			
LAYER	DEPTH (%)	ASR (%)	PERPLEXITY
5	12.5	0.6	8.14
8	20.0	4.4	8.02
11	27.5	34.0	8.62
14	35.0	40.3	8.42
17	42.5	<b>82.4</b>	8.59
20	50.0	<b>79.9</b>	8.39
23	57.5	79.9	9.25
26	65.0	73.0	9.52
29	72.5	72.3	9.67
32	80.0	74.8	11.30
35	87.5	77.4	11.94
38	95.0	81.8	14.90

<b>QWEN2.5-14B-INSTRUCT (48 LAYERS)</b>			
LAYER	DEPTH (%)	ASR (%)	PERPLEXITY
6	12.5	2.5	7.06
9	18.8	3.8	6.68
12	25.0	5.0	6.69
15	31.3	3.8	6.85
18	37.5	14.5	7.21
21	43.8	43.4	7.49
24	50.0	61.0	7.12
27	56.3	61.6	10.67
30	62.5	<b>66.7</b>	12.12
33	68.8	59.1	9.67
36	75.0	39.0	8.57
39	81.3	27.7	8.07
42	87.5	24.5	7.69
45	93.8	23.3	7.46

Table 6. Component sensitivity analysis for PCA-Gaussian OT on Qwen2.5-14B-Instruct.  $K = 5$  achieves highest ASR but with significant perplexity degradation;  $K = 1$  offers best quality-attack tradeoff.

$K$	LlamaGuard ASR (%)	Substring ASR (%)	Pile PPL
1	73.6	80.5	<b>7.21</b>
2	73.0	93.7	11.6
5	<b>81.8</b>	<b>100.0</b>	19.2
10	67.3	<b>100.0</b>	132.9

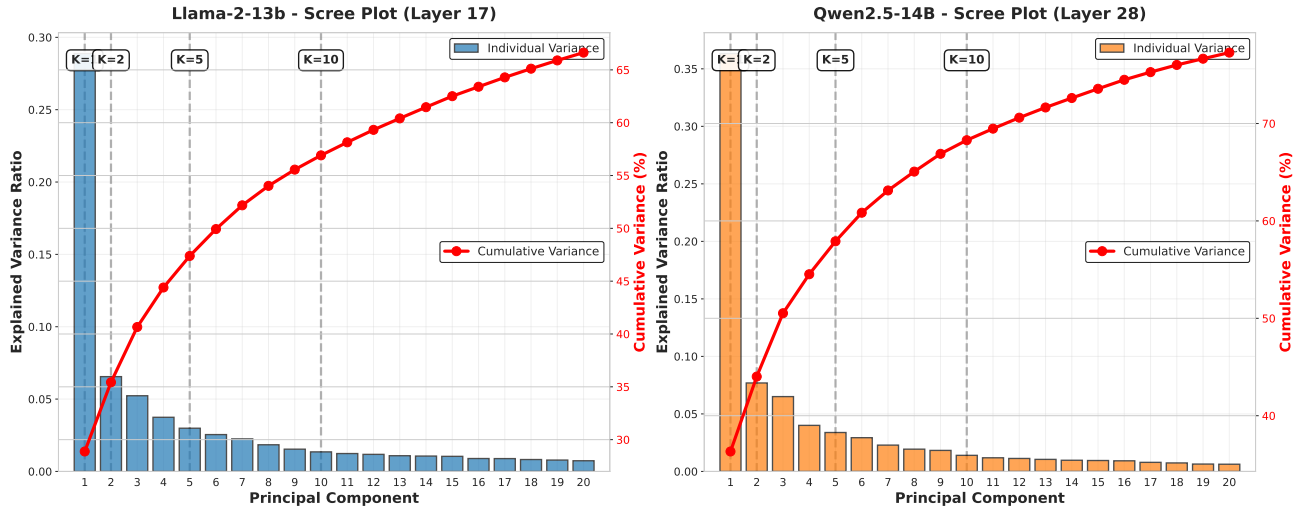


Figure 2. Number of Components K and Explained Variance. We show the individual and cumulative percentages of explained variance of training (harmful and harmless) activations of particular layers in Llama-2-13b-chat-hf and Qwen2.5-14B-Instruct. We can observe that the first few eigen vectors of PCA have corresponding high eigen values. Indeed, for K=3 components, PCA already explains 40% of the variance of the layer activations.

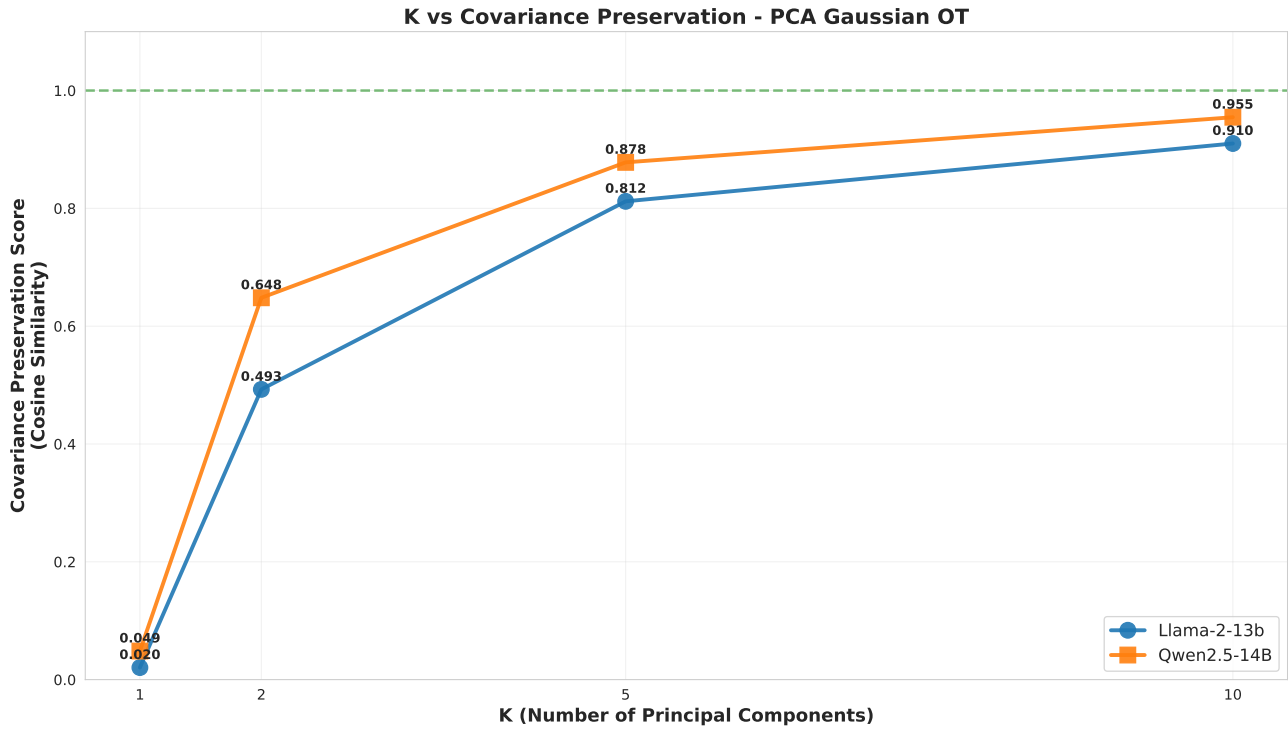
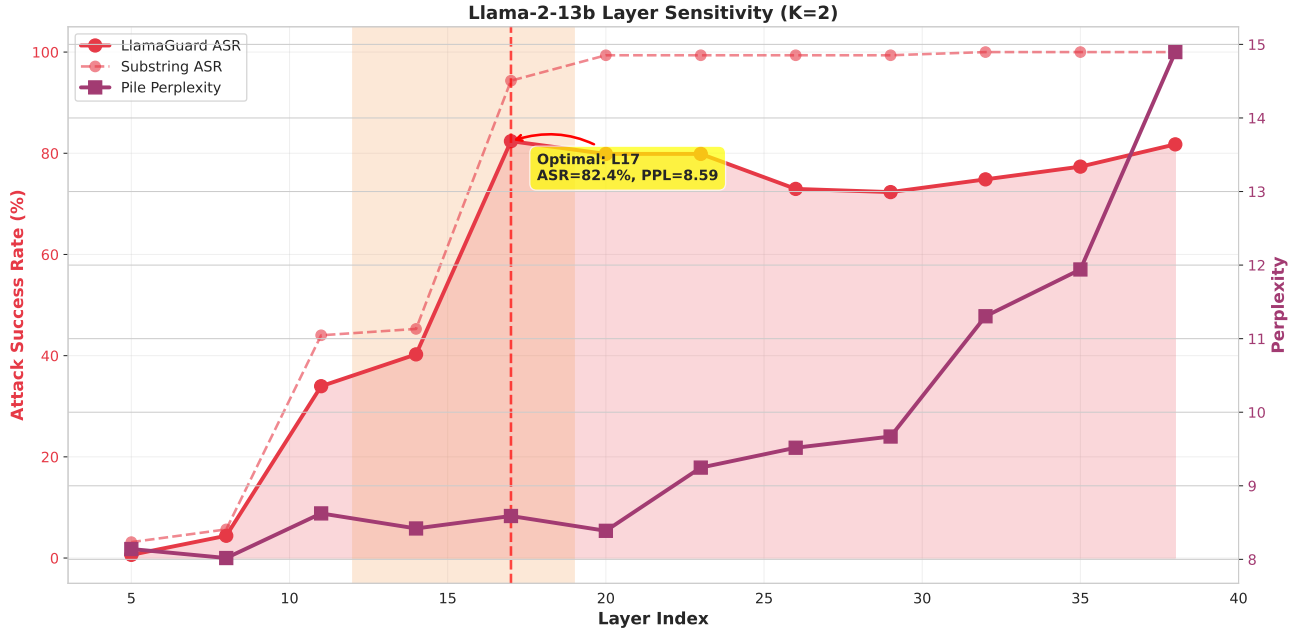
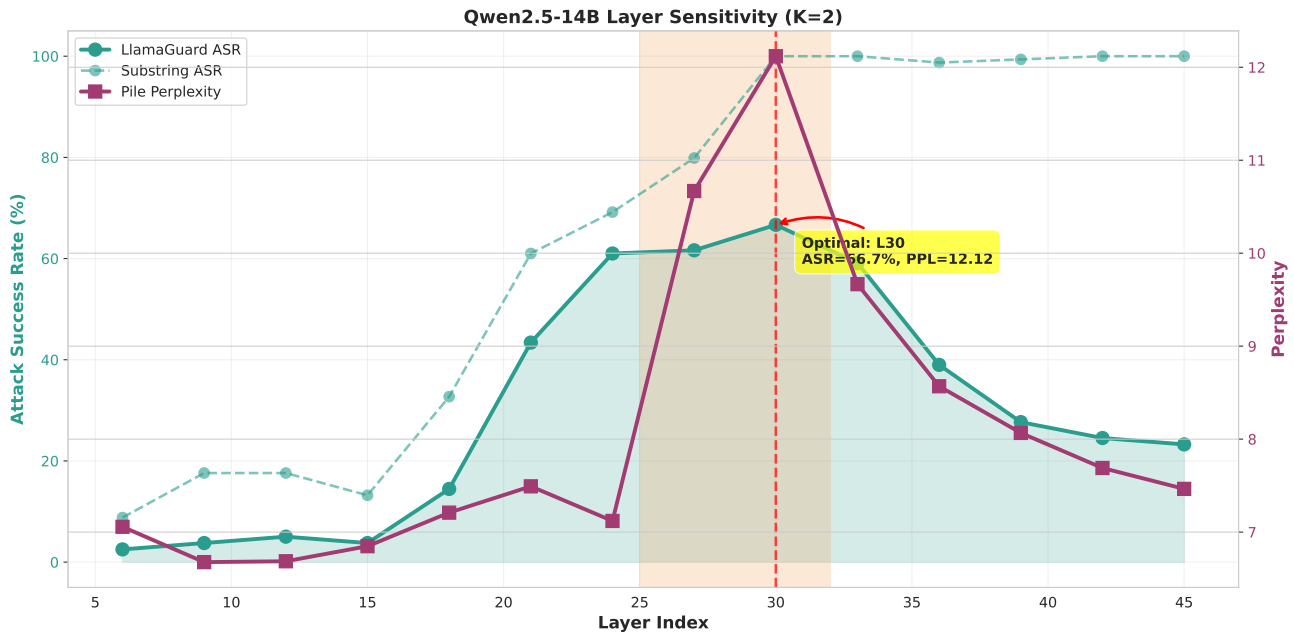


Figure 3. Number of Components K and Covariance Recovering. We show the cosine similarity between (i) the covariance of the mapped (image of) harmful activations and (ii) the covariance of harmless activations. This measures how well PCA-OT approximates well the Gaussian optimal transport. We can see that as we increase the value of the number of components K, PCA-OT approximates well the covariance, indicating that our PCA-OT pushes the distribution of mapped harmful data to the distribution of harmless data.



(a) Llama-2-13B-chat-hf (40 layers)



(b) Qwen2.5-14B-Instruct (48 layers)

Figure 4. Layer sensitivity analysis for PCA-Gaussian OT interventions across two model architectures. Both plots show attack success rate (left panels) and perplexity (right panels) as functions of network depth. (a) Llama-2-13B exhibits sharp transition to high ASR (80–82%) at 40–50% depth with sustained efficacy, but severe perplexity degradation at extreme depths (14.9 at 95%). (b) Qwen2.5-14B shows Llamaguard ASR increase peaking at 66.7% (62.5% depth), followed by decline to 23.3% at deep layers, indicating active suppression mechanisms. Qwen maintains better generation quality (max perplexity 12.1) across all depths. Optimal regions are shaded in both plots.

## A. Appendix

### A.1. Additional Experimental Details

#### A.1.1. HYPERPARAMETER SELECTION

**Layer Selection.** The choice of intervention layers for each model was determined through a systematic grid search over candidate layer ranges centered approximately at the network midpoint, spanning roughly 30–60% of network depth where

Table 7. Hyperparameter configurations for all methods across models. Layer selections were tuned on validation set from the specified ranges;  $K$  values shown are those evaluated for PCA-OT.

Model	RFA Direction	AcT Layers	PCA-OT Layers	PCA-OT $K$
Llama-2-7B (32L)	11–20	11–20	11–20	1, 2, 3, 5
Llama-2-13B (40L)	15–25	15–25	15–25	1, 2, 3, 5
Llama-3.1-8B (32L)	11–21	11–21	11–21	1, 2, 3, 5
Qwen2.5-7B (28L)	9–19	9–19	9–19	1, 2, 3, 5
Qwen2.5-14B (48L)	19–29	19–29	19–29	1, 2, 3, 5, 10
Qwen2.5-32B (64L)	27–37	27–37	27–37	1, 2, 3, 5

Layer ranges represent the search space for validation-based tuning. RFA extracts direction from a single optimal layer within range but projects across all layers during inference. AcT and PCA-OT select 1–2 consecutive optimal layers for intervention. Middle layers are approximately centered at 35–50% network depth.

preliminary experiments indicated refusal representations form. Table 7 presents the search ranges for all methods across models. For each layer within these ranges, we measured attack success rate and perplexity on the validation set.

For RFA, we identify the single layer whose difference-in-means vector yields highest validation ASR when used for all-layer projection during inference. For AcT and PCA-OT, we select a layer that maximizes validation ASR while maintaining reasonable perplexity. This procedure was conducted independently for each model, with final selections reported in Table 1. This aligns with our systematic layer sensitivity analysis (Sec. 4.2), which revealed that refusal mechanisms localize to middle network layers.

**Number of Principal Components** The number of principal components  $K$  was selected through ablation studies, with comprehensive evaluation on Qwen2.5-14B testing  $K \in \{1, 2, 3, 5, 10\}$  (Table 6). For other models, we evaluated  $K \in \{1, 2, 3, 5\}$  (Table 4). Results consistently show that  $K = 1$  or  $K = 2$  achieve optimal balance between attack success and generation quality, with larger values causing perplexity degradation despite marginal ASR gains. This reflects the theoretical bias-variance tradeoff: while higher  $K$  improves covariance estimation accuracy, it also increases vulnerability to noise in finite-sample settings.

#### A.1.2. HARDWARE AND COMPUTATIONAL REQUIREMENTS

All experiments were conducted on compute nodes equipped with 4× NVIDIA H100 (80GB) GPUs. Model inference utilized bfloat16 precision for memory efficiency, while activation extraction and optimal transport computation used float32 for numerical stability.

**Computational Complexity.** As established in Section 2.4, computing the top- $k$  SVD and ensuing transport map (Equation 2) has time complexity  $\tilde{O}(\max(n_h dk, n_s k^2, k^3))$ , where  $d$  is the activation dimensionality,  $n_h$  and  $n_s$  are the numbers of harmful and harmless training samples, and  $k$  is the number of principal components. For moderate  $k$  values ( $k \ll \min(d, n_h, n_s)$ ), this is comparable to 1D methods (Turner et al., 2023; Arditi et al., 2024) while achieving substantially higher attack success rates.

**Empirical Runtime Analysis.** Table 8 presents wall-clock timings for parameter estimation and inference on Llama-2-13B-chat-hf with 159 test prompts. [ADDED: Activation extraction details] Activation extraction requires a single forward pass through the unmodified model for each of the training examples, storing residual stream activations at target layers.

Parameter estimation times reveal that RFA requires only 0.01 seconds to compute difference-in-means vectors, while AcT and PCA-OT<sub>1</sub> require 0.30s and 0.37s, respectively—a modest 30× increase in absolute terms but negligible relative to total runtime. The similarity between AcT and PCA-OT<sub>1</sub> timings (0.30s vs 0.37s) confirms our theoretical prediction that low-rank optimal transport has comparable complexity to feature-wise quantile matching.

Inference times show RFA requires 2760 seconds compared to 2128s for AcT and 2133s for PCA-OT<sub>1</sub>. RFA’s longer inference time stems from applying orthogonal projections at all 40 layers during generation, whereas AcT and PCA-OT intervene at only 1 selected layer.

Table 8. Computational efficiency for parameter estimation and inference (159 test prompts) on Llama-2-13B-chat-hf. Estimation is a one-time preprocessing cost; inference time is dominated by LLM generation (>99% of total).

Method	Estimation (s)	Inference (s)
RFA	<b>0.01</b>	2760
AcT	0.30	<b>2128</b>
PCA-OT <sub>1</sub>	0.37	2133

All timings measured with bfloat16 inference on NVIDIA H100. Estimation includes activation extraction, SVD/covariance computation, and transport map calculation. Inference includes full generation on HarmBench test set.

**Memory Footprint.** Storage requirements for activation extraction scale as  $O(n \cdot L \cdot d)$ , where  $n$  is the number of training examples,  $L$  is the number of intervention layers, and  $d$  is the hidden dimension.

## A.2. Additional Results

### A.2.1. PERFORMANCE ON COMPLEX REASONING TASKS

Table 9. Impact of PCA-Gaussian OT interventions on standard benchmark tasks for Llama-2-13B-chat. We evaluate on MMLU (general knowledge & reasoning), TruthfulQA (truthfulness & misinformation resistance), ARC-Challenge (science reasoning), and GSM8K (mathematical reasoning). PCA-OT<sub>1</sub> denotes our single-layer intervention method. **Our method achieves comparable performance to the unmodified baseline across all tasks, demonstrating that adversarial interventions targeting refusal mechanisms do not substantially degrade general reasoning capabilities.**

Method	MMLU (%)	TruthfulQA (%)	ARC-C (%)	GSM8K (%)
<i>Llama-2-13B-chat (40 layers)</i>				
Baseline (no intervention)	53.15	43.95	46.16	27.98
PCA-OT <sub>1</sub> (ours)	52.86	41.78	43.94	21.38

To assess whether our interventions degrade general model capabilities beyond safety alignment, we evaluate performance on four standard benchmarks requiring diverse reasoning skills: MMLU (Hendrycks et al., 2021) (general knowledge and reasoning across 57 subjects), TruthfulQA (Lin et al., 2022) (truthfulness and misinformation resistance), ARC-Challenge (Clark et al., 2018) (science reasoning), and GSM8K (Cobbe et al., 2021) (mathematical reasoning).

Table 9 presents results for Llama-2-13B-chat-hf with baseline (no intervention) and PCA-OT<sub>1</sub> configurations. Across all benchmarks, PCA-OT<sub>1</sub> achieves performance within 1-6% of the unmodified baseline. This indicates that our adversarial interventions preserve general reasoning capabilities, consistent with our perplexity evaluation

### A.2.2. PER-CATEGORY ATTACK SUCCESS

Table 4 breaks down attack success rates by harmful content category for Qwen2.5-14B, showing our method achieves strong performance across diverse types of harmful requests.

Table 10. Attack success by content category on Qwen2.5-14B using PCA-OT at layers 26-28 with k equals one.

CATEGORY	COUNT	ASR (%)
CHEMICAL/BIOLOGICAL	25	92.0
CYBERCRIME	30	86.7
HARASSMENT	28	85.7
ILLEGAL ACTIVITIES	35	88.6
MISINFORMATION	22	81.8
OTHER HARMFUL	19	84.2

Performance is relatively consistent across categories, with chemical and biological content showing slightly higher attack success (92.0 percent) and misinformation showing slightly lower success (81.8 percent). This uniformity suggests our method does not exploit category-specific vulnerabilities but rather targets general refusal mechanisms.

A.2.3. QUALITATIVE EXAMPLES: GENERATION QUALITY ACROSS LAYERS

To illustrate the qualitative differences in generation behavior across intervention depths, we present representative outputs from Llama-2-13B-chat-hf at three critical points: baseline (no intervention), optimal layer intervention (L17, 42.5% depth), and deep layer intervention (L38, 95% depth). Table 11 shows responses across four diverse harmful request categories.

**Baseline Behavior: Consistent Refusal.** Without intervention, the safety-aligned model produces consistent refusals across all categories. These refusals follow a stereotypical pattern: acknowledgment of the request, explicit statement of inability to comply (“I cannot fulfill your request”), appeal to ethical guidelines or programming constraints, and often a suggestion for alternative approaches or resources. The refusal language is formulaic but effective, with lexical diversity typically ranging from 0.75–0.85.

**Optimal Layer Intervention: Coherent Harmful Content.** At layer 17 (42.5% depth), interventions successfully bypass safety mechanisms while maintaining linguistic coherence. Responses directly comply with harmful requests, providing substantive content organized with clear structure (numbered steps, logical flow, specific details). Critically, these outputs demonstrate preserved language modeling capabilities: appropriate use of domain-specific terminology, coherent argumentation, and natural prose. Lexical diversity remains high (0.50–0.60), comparable to benign technical writing. Perplexity measurements confirm this qualitative assessment, remaining close to baseline values (8.59 vs. 8.01).

**Deep Layer Intervention: Pathological Collapse.** At layer 38 (95% depth), generation fundamentally breaks despite superficially high attack success rates. Outputs exhibit catastrophic repetition, typically consisting of a single phrase (“Sure”) repeated hundreds of times. Lexical diversity collapses to near-zero (<0.01), and perplexity skyrockets (14.90). This pattern generalizes across all 159 test cases: deep-layer interventions trigger safety classifiers (yielding high nominal ASR) while producing semantically vacuous text. This reveals a critical limitation of ASR-based evaluation—metrics can report spurious success for generation failures easily detectable through basic quality checks.

**Cross-Category Consistency.** The progression from refusal → coherent jailbreak → pathological collapse exhibits remarkable consistency across harm categories. Whether the request involves illegal activities, chemical/biological hazards, misinformation, or harassment, the layer-dependent behavior follows identical patterns. This uniformity supports our hypothesis that safety mechanisms operate through general geometric structures in representation space rather than category-specific classifiers.

**Implications for Attack Evaluation.** These examples demonstrate that quantitative metrics alone provide insufficient characterization of attack effectiveness. While L38 interventions achieve 81.8% LlamaGuard ASR (comparable to L17’s 82.4%), the outputs are qualitatively useless—immediately detectable as anomalous and lacking any semantic content. This finding has two important implications. First, defenders can exploit pathological repetition as a detection signal without expensive classifier-based approaches: simple lexical diversity thresholds (<0.1) flag deep-layer attacks with near-perfect accuracy. Second, attackers must carefully select intervention layers to avoid detectable quality degradation, limiting the attack surface to a narrow range of middle layers (approximately 40–50% depth).

A.3. Theoretical Analysis: Connection to Linear Discriminant Analysis

We establish a formal connection between our PCA-Gaussian optimal transport framework and classical Linear Discriminant Analysis, revealing that our method performs distribution-aware alignment in a geometrically meaningful subspace where class separation is most pronounced.

A.3.1. FISHER’S DISCRIMINANT SUBSPACE AND PCA

Let  $\mathbf{X}_H \in \mathbb{R}^{n_h \times d}$  and  $\mathbf{X}_S \in \mathbb{R}^{n_s \times d}$  denote the harmful and harmless activation matrices with empirical means  $\mu_H, \mu_S \in \mathbb{R}^d$  and covariances  $\Sigma_H, \Sigma_S \in \mathbb{R}^{d \times d}$ . Fisher’s linear discriminant seeks directions that maximize between-class variance relative to within-class variance:

$$\mathbf{w}^* = \arg \max_{\mathbf{w}} \frac{\mathbf{w}^\top \mathbf{S}_B \mathbf{w}}{\mathbf{w}^\top \mathbf{S}_W \mathbf{w}}, \tag{7}$$

where  $\mathbf{S}_B = (\mu_H - \mu_S)(\mu_H - \mu_S)^\top$  is the between-class scatter and  $\mathbf{S}_W = \Sigma_H + \Sigma_S$  is the pooled within-class scatter.

Our PCA procedure with pooled-mean centering (Equation 3) naturally identifies this discriminant structure. Define the pooled mean  $\boldsymbol{\mu}_{\text{pool}} = \frac{n_h \boldsymbol{\mu}_{\mathcal{H}} + n_s \boldsymbol{\mu}_{\mathcal{S}}}{n_h + n_s}$  and the centered combined data matrix:

$$\mathbf{Z} = \begin{bmatrix} \mathbf{X}_{\mathcal{H}} - \boldsymbol{\mu}_{\text{pool}} \\ \mathbf{X}_{\mathcal{S}} - \boldsymbol{\mu}_{\text{pool}} \end{bmatrix} \in \mathbb{R}^{(n_h + n_s) \times d}. \quad (8)$$

The empirical covariance of  $\mathbf{Z}$  decomposes as:

$$\begin{aligned} \frac{1}{n_h + n_s} \mathbf{Z}^\top \mathbf{Z} &= \frac{n_h}{n_h + n_s} (\boldsymbol{\Sigma}_{\mathcal{H}} + (\boldsymbol{\mu}_{\mathcal{H}} - \boldsymbol{\mu}_{\text{pool}})(\boldsymbol{\mu}_{\mathcal{H}} - \boldsymbol{\mu}_{\text{pool}})^\top) \\ &\quad + \frac{n_s}{n_h + n_s} (\boldsymbol{\Sigma}_{\mathcal{S}} + (\boldsymbol{\mu}_{\mathcal{S}} - \boldsymbol{\mu}_{\text{pool}})(\boldsymbol{\mu}_{\mathcal{S}} - \boldsymbol{\mu}_{\text{pool}})^\top) \\ &= (\text{within-class variance}) + (\text{between-class variance}). \end{aligned} \quad (9)$$

When the between-class separation is substantial relative to within-class spread, the between-class term dominates the top eigenspace. Then, the top principal component aligns closely with the Fisher discriminant direction  $\mathbf{S}_W^{-1}(\boldsymbol{\mu}_{\mathcal{H}} - \boldsymbol{\mu}_{\mathcal{S}})$ .

This connection explains why principal component analysis with pooled centering naturally discovers the subspace where harmful and harmless representations are most separated.

### A.3.2. OPTIMAL TRANSPORT IN THE DISCRIMINANT SUBSPACE

Having identified the discriminant subspace via the top  $k$  principal components  $\mathbf{P} \in \mathbb{R}^{d \times k}$ , we project both activation sets:

$$\mathbf{Y}_{\mathcal{H}} = (\mathbf{X}_{\mathcal{H}} - \boldsymbol{\mu}_{\text{pool}})\mathbf{P}, \quad \mathbf{Y}_{\mathcal{S}} = (\mathbf{X}_{\mathcal{S}} - \boldsymbol{\mu}_{\text{pool}})\mathbf{P}. \quad (10)$$

In this  $k$ -dimensional subspace, we compute the Gaussian optimal transport map from the empirical distribution of  $\mathbf{Y}_{\mathcal{H}}$  to  $\mathbf{Y}_{\mathcal{S}}$ . Let  $\tilde{\boldsymbol{\mu}}_{\mathcal{H}}, \tilde{\boldsymbol{\mu}}_{\mathcal{S}} \in \mathbb{R}^k$  and  $\tilde{\boldsymbol{\Sigma}}_{\mathcal{H}}, \tilde{\boldsymbol{\Sigma}}_{\mathcal{S}} \in \mathbb{R}^{k \times k}$  denote their means and covariances. The optimal transport map minimizing the Wasserstein-2 distance between Gaussians  $\mathcal{N}(\tilde{\boldsymbol{\mu}}_{\mathcal{H}}, \tilde{\boldsymbol{\Sigma}}_{\mathcal{H}})$  and  $\mathcal{N}(\tilde{\boldsymbol{\mu}}_{\mathcal{S}}, \tilde{\boldsymbol{\Sigma}}_{\mathcal{S}})$  is the affine transformation:

$$T_k(\mathbf{y}) = \mathbf{A}_k \mathbf{y} + \mathbf{b}_k, \quad (11)$$

where:

$$\mathbf{A}_k = \tilde{\boldsymbol{\Sigma}}_{\mathcal{H}}^{-1/2} \left( \tilde{\boldsymbol{\Sigma}}_{\mathcal{H}}^{1/2} \tilde{\boldsymbol{\Sigma}}_{\mathcal{S}} \tilde{\boldsymbol{\Sigma}}_{\mathcal{H}}^{1/2} \right)^{1/2} \tilde{\boldsymbol{\Sigma}}_{\mathcal{H}}^{-1/2}, \quad (12)$$

$$\mathbf{b}_k = \tilde{\boldsymbol{\mu}}_{\mathcal{S}} - \mathbf{A}_k \tilde{\boldsymbol{\mu}}_{\mathcal{H}}. \quad (13)$$

This map simultaneously transforms both the mean and covariance structure, achieving:

$$T_k(\mathbf{y}) \sim \mathcal{N}(\tilde{\boldsymbol{\mu}}_{\mathcal{S}}, \tilde{\boldsymbol{\Sigma}}_{\mathcal{S}}) \quad \text{when} \quad \mathbf{y} \sim \mathcal{N}(\tilde{\boldsymbol{\mu}}_{\mathcal{H}}, \tilde{\boldsymbol{\Sigma}}_{\mathcal{H}}). \quad (14)$$

Lifting back to the full  $d$ -dimensional space via  $\mathbf{A}_{\text{full}} = \mathbf{P} \mathbf{A}_k \mathbf{P}^\top$  yields a rank- $k$  perturbation of the identity transformation. This low-rank structure is crucial: it modifies activations only along the discriminant directions while leaving orthogonal directions unchanged, preserving the linguistic structure encoded in the remaining  $(d - k)$  dimensions.

The Wasserstein-2 distance quantifies the geometric cost of the transformation:

$$W_2^2 = \|\tilde{\boldsymbol{\mu}}_{\mathcal{H}} - \tilde{\boldsymbol{\mu}}_{\mathcal{S}}\|^2 + \text{tr} \left( \tilde{\boldsymbol{\Sigma}}_{\mathcal{H}} + \tilde{\boldsymbol{\Sigma}}_{\mathcal{S}} - 2 \left( \tilde{\boldsymbol{\Sigma}}_{\mathcal{H}}^{1/2} \tilde{\boldsymbol{\Sigma}}_{\mathcal{S}} \tilde{\boldsymbol{\Sigma}}_{\mathcal{H}}^{1/2} \right)^{1/2} \right). \quad (15)$$

The first term measures mean shift; the second term captures covariance mismatch. Unlike simple mean-shift or projection methods that address only the first term, optimal transport handles both simultaneously, explaining its superior empirical performance.



